*ILASS–Europe 2017, 28th Conference on Liquid Atomization and Spray Systems, 6-8 September 2017, Valencia, Spain*
*http://dx.doi.org/10.4995/ILASS2017.2017.4742*

# Quantification of diesel injector dribble using 3D reconstruction from x-ray and DBI imaging

Vitaliy Sechenyh[1], Jack Turner[1], Dan Sykes[1], Daniel J. Duke[2], Andrew B. Swantek[2], Katarzyna E. Matusik[2], Alan L. Kastengren[2], Christopher F. Powell[2], Alberto Viera[3], Raul Payri[3], Cyril Crua[1,*]
[1]Advanced Engineering Centre, University of Brighton, Brighton, UK
[2]Argonne National Laboratory, USA
[3]CMT Motores Térmicos - Universitat Politècnica de València, Spain
*corresponding author: c.crua@brighton.ac.uk

**Abstract**
Post-injection dribble is known to lead to incomplete atomisation and combustion due to the release of slow moving, and often surface-bound, liquid fuel after the end of the injection event. This can have a negative effect on engine emissions, performance, and injector durability. To better quantify this phenomenon we present a new image processing approach to quantify the volume and surface area of ligaments produced during the end of injection, for an ECN 'Spray B' 3-hole injector. Circular approximation for cross-sections was used to estimate three-dimensional parameters of droplets and ligaments. The image processing consisted in three stages: edge detection, morphological reconstruction, and 3D reconstruction. For the last stage of 3D reconstruction, smooth surfaces were obtained by computation of the alpha shape which represents a bounding volume enveloping a set of 3D points. The object model was verified by calculation of surface area and volume from 2D images of figures with well-known shapes. We show that the object model fits non-spherical droplets and pseudo-cylindrical ligaments reasonably well. We applied our processing approach to datasets generated by different research groups to decouple the effect of gas temperature and pressure on the fuel dribble process. High-speed X-ray phase-contrast images obtained at room temperature conditions (297 K) at the 7-ID beamline of the Advanced Photon Source at Argonne National Laboratory, together with diffused back-illumination (DBI) images captured at a wide range of temperature conditions (293-900 K) by CMT Motores Térmicos, were analysed and compared quantitatively.

**Keywords**
Diesel injector; dribble; ligament; droplet shape; atomisation.

## Introduction

The end-of-injection (EOI) fuel dribble causes a formation of unburned hydrocarbons and decreases the performance of internal combustion engines in a variety of ways. For example, deposits lead to an increase in air pollutant emissions [1, 2], a decrease in quality of injection [2, 3, 4] and further coking of the nozzle [5]. Understanding of the fuel dribbling process is particularly important for the development of a strategy for optimal use of fuels. However, observing the transient end-of-injection processes is particularly challenging due to the extreme operating conditions and the microscopic scales involved. Consequently, there is a lack of quantitative information on the fuel dribble events and the parameters that affect them.

Recently published studies [6-10] demonstrate different aspects of the EOI fuel dribble based on a qualitative and quantitative analysis of experimental images of the injection process. The following important factors affecting the mechanism of the fuel dribble were studied: peak injection velocity [7], needle closing speed [7], in-cylinder pressure [6, 7], injection pressure [6], fuel mass expulsion [9], bubble ingestion at the EOI [10], liquid length recession at the EOI [8] and different flow characteristics at the EOI [11].

The present study is dedicated to a quantitative analysis of the fuel dribble with the focus on dribble volumes estimated by processing of images from high-speed X-ray phase-contrast and diffused back-illumination (DBI) imaging techniques. The 3D reconstruction algorithm was developed to analyse volumes of the liquid when the fuel emerges from the orifice of Engine Combustion Network (ECN) "Spray B" injector. The main motivation of this investigation is to provide a better understanding of the parameters that influence the uncontrolled release of low velocity fuel at the end of injection.


EDITORIAL UNIVERSITAT POLITÈCNICA DE VALÈNCIA

**3D reconstruction algorithm**

The extraction of size and shape from two-dimensional images of droplets, particles, liquid ligaments or tree-like structures is used in a number of industrial applications such as medical imaging [12-15], soot formation in combustion [16], etc. Similar to previously published algorithms [17-19], the present analysis is based on the estimation of object cross-sections from a line-based structure of an initial image followed by smoothing of 3D shape. The present study is based on the object model demonstrated in Fig. 1a. A circular assumption for object cross-sections allowed to reconstruct the 3D shape using the limited information available from a single 2D image.

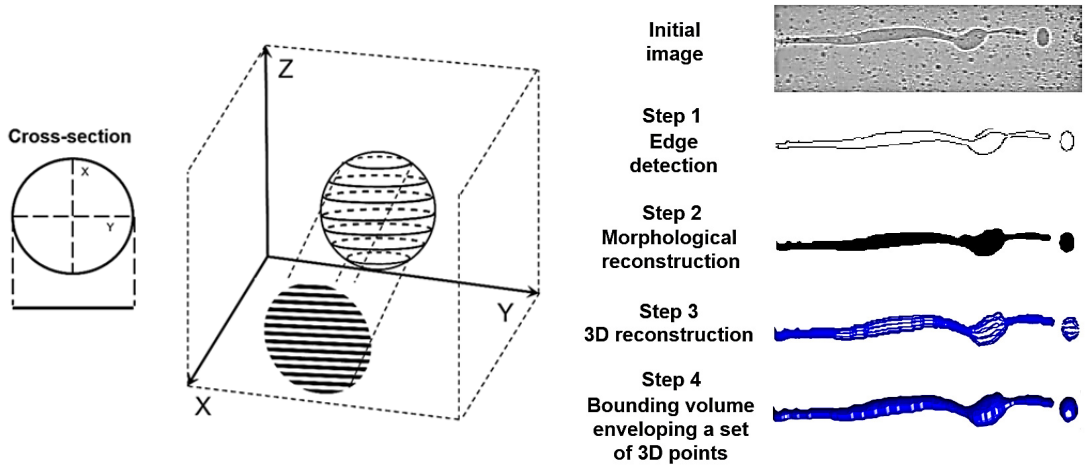


**Figure 1.** Schematic of the object model (a) and main steps of the image processing algorithm (b).

The image processing algorithm consisted of the following stages (see Fig. 1b):

- Step 1. Edge detection coupled with conversion from grey scale to binary image.
- Step 2. Morphological reconstruction of contours for all detected objects. Intermediate stage: Line-based structure of binary image is used to calculate characteristics of object cross-sections.
- Step 3. 3D reconstruction. Coordinates of 3D points are calculated based on centres and radii of cross-sections.
- Step 4. Computation of the bounding volume which envelops a set of 3D points – alpha shape.

The present study applies this image processing approach to two different experimental techniques: high-speed x-ray phase contrast and diffused back-illumination (DBI). Three different edge detection methods were used to remove background and noise from experimental images: Canny algorithm [20], wavelet filter and morphological opening.

A choice of the Canny edge detector is motivated by its excellent performance in the presence of flickering background and boundaries which are caused by a combination of X-ray absorption and phase contrast effects [21, 22]. Since detected edges usually have breaks, a Delaunay triangulation algorithm [23] was applied for two-dimensional reconstruction of contours of multiple objects. Compared to the X-ray imaging, the DBI method provides similar light intensity values for each pixel which belongs to the liquid phase [24]. DBI pictures were processed with help of a transformation which consists of a convolution of the image with a wavelet filter, followed by a thresholding. The wavelet filter detects concavity and convexity of the grey level variation in the image [25]. Edges from DBI images were also detected by morphological opening with erosion followed by a dilation, using the same structuring element for both operations. Details related to the application of morphological operations to greyscale images were discussed elsewhere in the literature [25, 26]. Following recommendations in the literature [25, 26, 28, 29, 30], the adjustable parameters for each edge detection method were chosen depending on a number factors: size and number of objects, type of a background noise, movements of the image background and image contrast.

The intermediate stage of the image processing algorithm uses line-based structure of binary images with contours of objects. The detection of grouped pixels in single lines of images was used to determine diameters and coordinates of centres for all detected circles. A middle point and a number of grouped pixels were accepted as centre and diameter of circles, respectively.

Previously determined characteristics together with a parametric equation for a circle are used to build a 3D point cloud for each cross-section (slice) of the object, in a plane orthogonal to the image plane. Merging all available "slices" generates a 3D array which represents the shape of the object. At the last stage of 3D reconstruction, a smooth surface is obtained by computation of the bounding volume enveloping the 3D point cloud – the alpha shape. The definition of the alpha shape in three-dimensional space was discussed in the literature by Edelsbrunner et al. [31].

There are three main parameters necessary to build the alpha shape: alpha radius, region threshold and holes threshold. Depending on a value of the alpha radius, the alpha shape can transform from concave into convex object. Larger values of alpha radius usually result in convex objects. Lafarge et al. [32] provide recommendations for the choice of the alpha radius which are necessary for correct representation of the 3D shape. The region threshold allows the maximum number of objects in the 3D array to be determined. Finally, holes threshold reduces the number of defects and holes in the alpha shape.

**Verification of the 3D reconstruction algorithm**

The 3D reconstruction algorithm was verified by calculation of surface area ($S$) and volume ($V$) from 2D images of figures with well-known shapes: sphere, cylinder, and spheroid. The average relative error was chosen as a measure of accuracy in calculation of $S$ and $V$. The description of test shapes and errors are summarized in Table 1. A cylinder, spheres, and prolate and oblate spheroids were considered as models for liquid ligaments and droplets. Two half-spheres were attached to the cylinder in order to model a typical shape of the ligament.

Average relative errors in calculations of $V$ and $S$ for spherical objects are 4.7% and 3.4 %, respectively. Inclined spheroids were chosen to simulate the rotation of ligaments in images of the fuel dribble. As is seen in Table 1, the largest relative error in calculations of $V$ and $S$ is observed in cases when the inclination angle of the major axis of the spheroid ($A$) equals 129 degrees. It should be mentioned that the most accurate reconstruction of the 3D shape was observed for the object with a vertically oriented major axis – a cylinder with two hemispherical caps.

Two spheres with different distances between their centres were chosen as models of the pinch-off effect. Current analysis showed that the change of the distance between two spheres produces errors which equal 19% and 5.9% for $V$ and $S$, respectively. In addition, a combination of prolate spheroid and sphere was also considered as the model for the initial stage of the pinch-off effect.

**Table 1.** Average relative error in calculations of volume and surface area for different test shapes

| Description of test shapes | Volume error (%) | Surface area error (%) |
|---|---|---|
| Sphere | 4.7 | 3.4 |
| Prolate spheroid. $A$=0° | 2.7 | 1.9 |
| Prolate spheroid. $A$=1° | 6.5 | 4.3 |
| Prolate spheroid. $A$=5° | 7.6 | 4.9 |
| Prolate spheroid. $A$=12° | 11 | 7.6 |
| Prolate spheroid. $A$=21° | 13 | 10 |
| Prolate spheroid. $A$=29° | 30 | 24 |
| Oblate spheroid. $A$=90° | 8.3 | 45 |
| Prolate spheroid and sphere | 16 | 6.4 |
| Cylinder with two hemispherical caps | 0.6 | 0.1 |
| Two spheres separated by 0.05$D$ | 14 | 0.8 |
| Two spheres separated by 0.15$D$ | 14 | 1.6 |
| Two spheres separated by 0.2$D$ | 19 | 5.9 |

For this initial approach at modelling the 3D morphology of microscopic droplets and ligaments we have made two simplifying assumptions: the liquid structures are axisymmetric, and aligned with the pixel array. While these assumptions preclude the 3D modelling of completely arbitrary shapes, they can be justified by the experimental configurations used in this particular study.

The assumption of axisymmetry can be justified by the fact that the experiments were performed with the spray axis aligned with the image plane, and both surface tension and momentum limit the formation of asymmetric liquid structures in the plane orthogonal to the spray axis. This is particularly the case when liquid velocities are small, which is to be expected for our experiments performed during the end of injection. Although this assumption cannot be easily verified since measurements for the depth of the fuel structures were not available, we note that this should be a reasonable hypothesis for the study of slow-moving ligaments and droplets.

The assumption that liquid structures are aligned with the pixel array was made to simplify the slice by slice reconstruction process. This assumption was satisfied by ensuring that the spray axis was aligned with the pixel array, either during the image acquisition or by rotation of the acquired images. The effect of rotation of spheroid structures with regard to the pixel array is quantified in Table 1, and as expected larger errors are obtained for angles that deviate from the images axes. It should be mentioned that such large errors are expected to be rare in this study, as the vast majority of ligaments were well aligned with the image (i.e. spray) axis.

**Results and discussion**

As mentioned previously, the present analysis uses pictures of EOI fuel dribble obtained by X-ray imaging and DBI. Both experimental techniques were already reported extensively [9, 10, 11, 21, 22, 24, 33], hence for conciseness the technical details of the experimental setup will not be repeated here. The main experimental parameters relevant to the study of the fuel dribble process are listed in Table 2.

**Table 2.** Summary of experimental conditions for datasets used for analysis of the EOI fuel dribble

| Experimental conditions | CMT | Argonne |
|---|---|---|
| Injected liquid | n-dodecane | n-dodecane |
| Injection pressure $P_{inj}$, [bar] | 500; 1000; 1500 | 500; 1000; 1500 |
| Ambient gas | 100% $N_2$ | 100% $N_2$; 82% $N_2$ +18% He (by mass) |
| Gas temperature $T_g$, [K] | 293 – 900 | 297 |
| Gas pressure $P_g$, [bar] | 6.7 – 62 | 14.4; 30 |
| Ambient gas density, [kg/m$^3$] | 7.6 – 30 | 16.5; 34 |

X-ray imaging of the fuel injection process was done at room temperature conditions at the 7-ID beamline of the Advanced Photon Source at Argonne National Laboratory (US). The exposure time and the pixel size were $1.473 \cdot 10^{-5}$ s and $5 \cdot 10^{-6}$ m square, respectively. A raw image and the result of the 3D reconstruction is shown in Fig. 2. The nozzle orifice is located above the top part of both pictures.

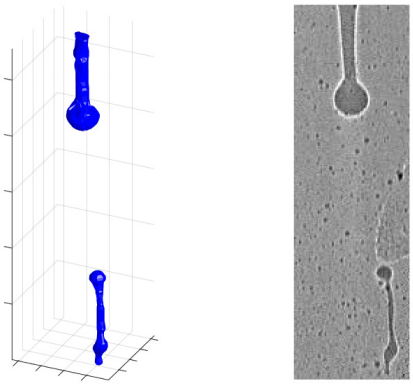

**Figure 2.** The raw image from X-Ray phase contrast technique (right image) and the result of 3D reconstruction (left image). Experimental conditions: $P_{inj}$=500 bar, $P_g$=30 bar and $T_g$=297 K.

DBI images were captured at the CMT Motores Térmicos (Spain) in two different sets of experimental measurements: room temperature (293 K) and high temperatures (473-900 K) conditions. The first image set was carried out with a LED pulse length (exposure time) of $1 \cdot 10^{-7}$ s and pixel sizes of $1.35 \cdot 10^{-5}$ m or $1.99 \cdot 10^{-5}$ m, depending on the optical magnification. An example of 3D reconstructed image is shown in Fig. 3. Similar to Fig. 2, the nozzle orifice is located just above the top of Fig. 3.

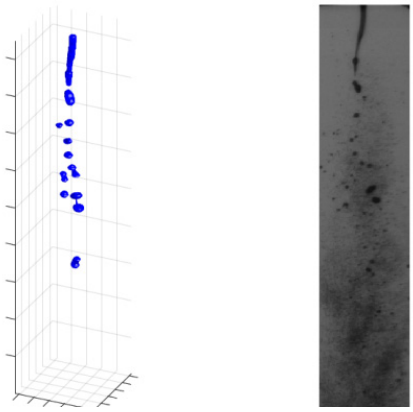

**Figure 3.** Room temperature DBI image (right image) and the result of 3D reconstruction (left image). Experimental conditions: $P_{inj}$=500 bar, $P_g$=27 bar and $T_g$=293 K.

The present analysis required the separation of the dribble events from the main injection stage, when a finely atomised spray is formed. As can be seen in Fig. 4, the liquid volume present in the region of interest increases rapidly at the beginning of the injection stage, and reduces almost to zero when the needle of the diesel injector closes (at 4.5 ms in Fig. 4). The volume of liquid present in the region of interest then increases again due to the dribble process. The image analysis shows that the relative duration of dribble events varied from 5 to 23 % of the time between opening and closing of the injector needle.

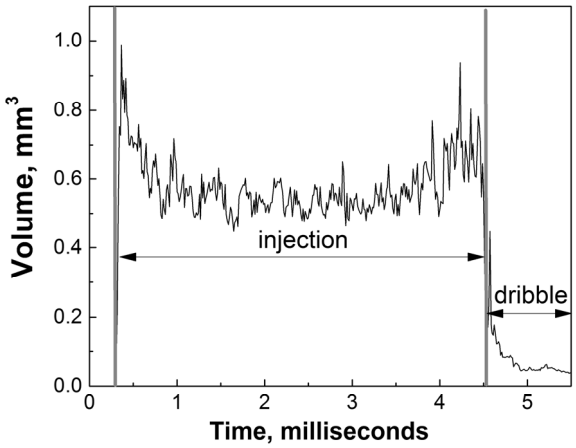


**Figure 4.** Time dependence of the liquid volume during the injection process for: $P_{inj}$=1500 bar, $T_g$=900 K and $P_g$=20 bar. Experimental images were provided by Argonne.

As is seen in Fig. 5, both the volume (*V*) and external surface area (*S*) of the liquid structures present in the region of interest increase rapidly to a maximum value before gradually decreasing to zero. Solid and dashed lines were included in Fig. 5 in order to provide a graphical representation of time evolution for *V* and *S*. All dribble events showed similar behaviour with respect to changes in liquid volume and surface area. The initial increases in V and S relate to the fuel being released from the orifice after the end of the main injection event. The decrease in these quantities is related to the disappearance of the structures from the region of interest, as they move out of the field of view of the imaging systems. Since all dribble image sequences demonstrated this behaviour, the maximum dribble volume was considered as a characteristic parameter of the process.

Firstly, we can note that the values for the maximum dribble volume obtained from the very different experiments performed by CMT and Argonne are in good quantitative agreement (see data at 293 – 297 K in Fig. 6), suggesting that the fuel volumes estimated from our morphological reconstructions are consistent. In agreement with previously published studies [6, 7], this investigation revealed a high cycle-to-cycle deviation in the quantity of fuel delivered after the end of injection. No clear dependence of the fuel dribble on injection pressure was observed (Fig. 6), although the lowest injection pressure tested (500 bar) seemed to generate relatively more dribble at room temperature conditions. As is seen in Fig. 6, the volume measurements for high gas temperature are less consistent, and as a result it is more difficult to identify a clear overall dependence of the fuel dribble on injection pressure. One may argue that fuel injection pressure should be expected to have no direct effect on the

release of fuel after the nozzle has been closed. At the same time, we should consider that higher injection pressures are known to lead to higher gas volume fractions in the nozzle (through cavitation), which in turn should reduce the volume of liquid trapped inside the nozzle and orifices after needle closure.

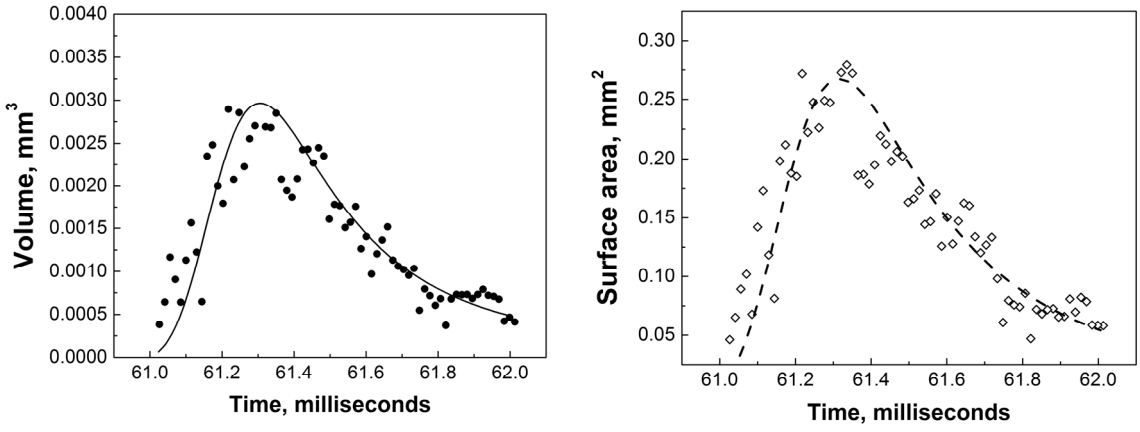


(a) (b)

**Figure 5.** Dribble volume (left image) and surface area (right image) versus time. Both diagrams obtained by processing of images which correspond to following conditions: $P_{inj}$=1000 bar, $T_g$=297 K and $P_g$=30 bar. Experimental images were provided by Argonne.

Our analysis shows that gas temperature has a significant impact on the volume of fuel dribble (Fig. 6). Measurements performed at elevated temperatures (473 – 900 K) were found to generate between 2 and 4 times more liquid after the end of the main injection event, for all injection pressures (Fig. 6). Interestingly, the largest volume of fuel dribble was recorded for mid-range temperatures (473 K). This may suggest that at room temperature the high viscosity of the liquid prevents some of the fuel from dribbling out of the nozzle. As the gas temperature is increased (and the viscosity and surface tension of the liquid reduced) a larger volume of fuel is able to flow out of the orifice. Since the dribble process is affected by momentum, it can also be expected that the lower gas densities obtained at high gas temperatures (for a fixed gas pressure) should lead to more fuel being released from the nozzle. As temperature is further increased to 820 – 900 K, the trend reverses and the measured dribble volume somewhat reduces (Figs. 6 and 7a), indicating that other parameters are affecting the process. We note that the apparent reduction in measured dribble volume at high temperatures could be related to increased evaporation at these conditions, rather than a net reduction in released liquid volume.

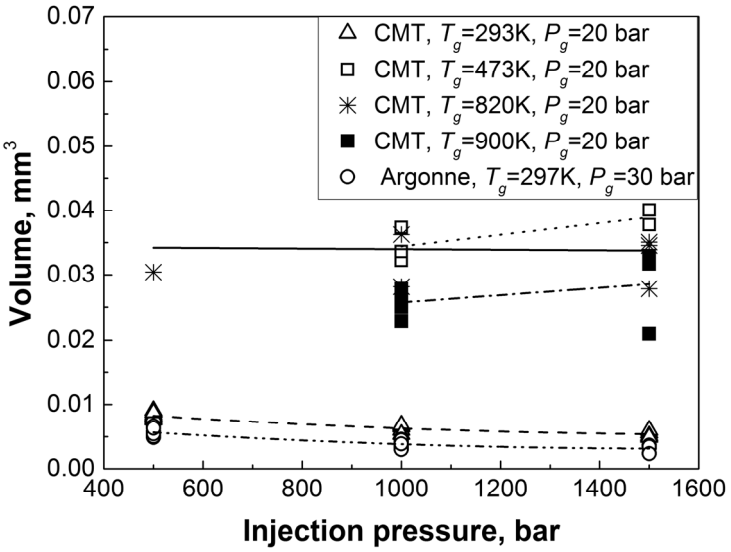


**Figure 6.** Dependence of maximum dribble volume on injection pressure $P_{inj.}$

The investigation shows that an increase in gas pressure reduces the volume of dribble (Fig. 7b). Again this behaviour is expected to be related to a reduction in gas density, providing less resistance to the flow of fuel out of the injector's orifices.

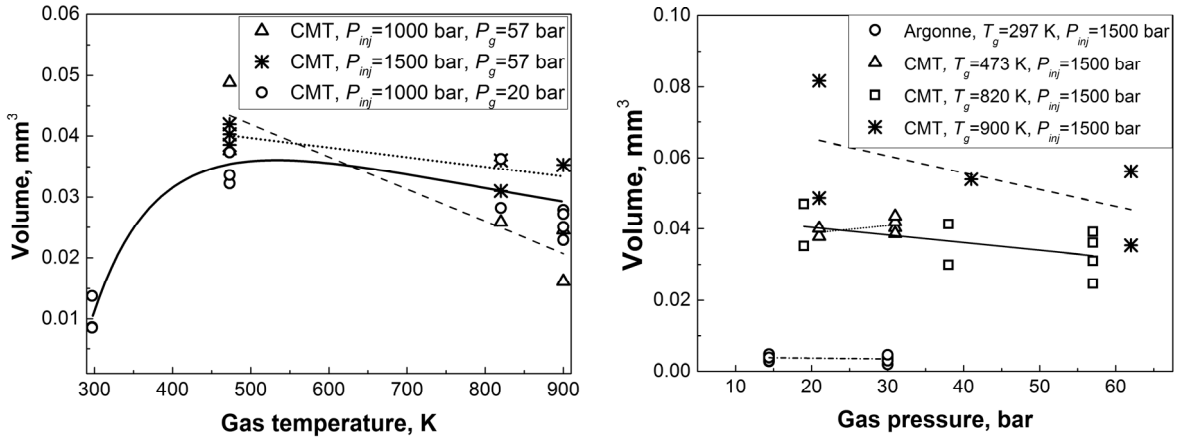


(a) (b)

**Figure 7.** Dependence of the maximum dribble volume on gas temperature $T_g$ (a) and pressure $P_g$ (b).

## Conclusions

We performed a quantitative investigation of fuel injector dribble using 3D morphological reconstruction of liquid structures using high-speed videos recorded at Argonne (X-ray phase-contrast) and CMT Motores Térmicos (diffused back-illumination). This allowed us to estimate the volume of liquid released from the orifice of an ECN "Spray B" injector after the end of injection. Our analysis showed that the duration of dribble events varied from 5 to 23 % of the injection time. We found that a larger volume of fuel dribble occurred at low injection pressures, mid-range gas temperatures (~473 K) and low gas pressures. Although a more detailed analysis would be needed to confirm these trends, it is interesting to note that these conditions are generally found at idle engine conditions.

## Acknowledgements

This work was supported by the UK's Engineering and Physical Science Research Council [grants EP/K020528/1 and EP/M009424/1], and BP Formulated Products Technology.

The authors acknowledge the support of this work from CMT Motores Térmicos (Universitat Politècnica de València, Spain). Parts of this research were performed at the 7-ID beam line of the Advanced Photon Source at Argonne National Laboratory. Use of the APS is supported by the U.S. Department of Energy (DOE) under Contract No. DEAC02-06CH11357. This research was partially funded by DOE's Vehicle Technologies Program, Office of Energy Efficiency and Renewable Energy. The authors would like to thank Team Leaders Gurpreet Singh and Leo Breton for their support of this work

## Nomenclature

| | |
|---|---|
| $T$ | temperature [K] |
| $P$ | pressure [bar] |
| $V$ | volume [m$^3$] |
| $S$ | surface area [m$^2$] |
| $D$ | diameter [m] |
| $A$ | angle [degrees] |

## References

[1] Sandquist, H., Denbratt, I., Owrang, F., Olsson, J., Influence of Fuel Parameters on Deposit Formation and Emissions in a Direct Injection Stratified Charge SI Engine, 2001, SAE Paper 2001-01-2028.

[2] Caprotti R., Fowler W.J., Diesel additive technology effects on injector hole erosion/corrosion, injector fouling and particulate traps, 1993, SAE Paper 932739.

[3] Lepperhoff G., Houben, M., Mechanisms of Deposit Formation in Internal Combustion Engines and Heat Exchangers, 1993, SAE Paper 931032.

[4] Birgel, A., Ladommatos, N., Aleiferis, P., Zülch, S., Milovanovic, N., Lafon, V., Orlovic, A., Lacey, P., Deposit Formation in the Holes of Diesel Injector Nozzles: A Critical Review, SAE Paper 2008-01-2383.

[5] Argueyrolles, B., Dehoux, S., Gastaldi, P., Grosjean, L., Levy, F., Michel, A., Passerel, D., Influence of injector nozzle design and cavitation on coking phenomenon, SAE Paper 2007-01-1896.
[6] Turner, J.E., Stetsyuk, V., Crua, C., Pearson, R.J. Gold, M.R., August 23-27 2015, 13th International Conference on Liquid Atomization and Spray Systems, Tainan, Taiwan.
[7] Moon, S., Huang, W., Li Z., Wang, J., 2016, Applied Energy, 179, pp.7-16.
[8] Kook, S., Pickett, L., Musculus, M., Influence of diesel injection parameters on end-of-injection liquid length recession, 2009, SAE Int. J. Engines, 2, pp. 1194-210.
[9] Swantek, A. B., Duke, D. J., Tilocco, F. Z., Sovis, N., Powell, C., Kastengren, A. L., 2014, ILASS-Americas 26th Annual Conference on Liquid Atomization and Spray Systems, Portland, Oregon
[10] Swantek, A. B., Kastengren, A. L., Duke, D. J., Tilocco, F., Sovis, N., Powell, C. F., 8-10 September, 2014, ILASS Europe, 26th Annual Conference on Liquid Atomization and Spray Systems, Bremen, Germany.
[11] Kastengren, A., Powell, C.F., Tilocco, F.Z., Liu, Z., Moon, S., Zhang, X., Gao, J., 2012, J. Eng. Gas Turbines Power, 134, p. 094501.
[12] Fessler, J. A., Macovski, A., 1991, IEEE Transactions on Medical Imaging 10, pp. 25-39.
[13] Kumar, S.S, Amutha, R., March 30-31, 2012, IEEE-International Conference On Advances In Engineering, Science And Management (ICAESM -2012).
[14] Cárdenes, R., Alexey, N., Julian, G., Rod H., Alejandro, F.F., 2012, IEEE International Symposium on Biomedical Imaging.
[15] Goyal, M., Prakash A., Yang, J., 2013. 3D Reconstruction of Coronary Arteries from Angiographic Images: A Survey.
[16] Sommer, H.J., Kao, C.C., Turns, S.R., 1990, 13th Annual Energy-Sources Technology Conference. Petroleum Division, The American Society of Mechanical Engineers, New York
[17] Kitamura K., Tobis J. M., Sklansky J., 1988, IEEE Truns. Med. Imaging, 7, pp. 173-187.
[18] Hoffmann K.R., Doi K., Chan H., Chua K., 1987, Proc. SPIE 767, Med. Imaging, pp. 449-453.
[19] Colombo C., Bimbo A., Pernici F., 2005, IEEE transactions on pattern analysis and machine intelligence, 27, 1, pp.99-144.
[20] Canny, J., A Computational Approach to Edge Detection, 1986, IEEE Transactions on Pattern Analysis and Machine Intelligence, PAMI-8, 6, pp. 679-698.
[21] Duke, D. J., Swantek, A., Tilocco, Z., Kastengren, A., Fezzaa, K., Neroorkar, K., et al., 2014, SAE Int. J. Engines, 7(2), pp. 1003-1016.
[22] Kastengren, A. L., Tilocco, F., Duke, D. J., Powell, C., Zhang, X., & Moon, S., 2014, Atomization and Sprays, 24, 3, pp. 251-272.
[23] Delaunay, B., 1934, Bulletin de l'Académie des Sciences de l'URSS, Classe des sciences mathématiques et naturelles, 6, pp. 793-800.
[24] Pauri, R., Bracho, G., Gomes-Aldaravi, P.M., Viera, A., 2017, Atomization and Sprays, DOI: 10.1615/AtomizSpr.2017017949.
[25] Nicolas Fdida, Développement d'un système de granulométrie par imagerie: application aux sprays larges et hétérogènes, 2008, pp. 71-76.
[26] Serra, J., 1983, Image Analysis and Mathematical Morphology. Academic Press, Inc., Orlando, FL, USA.
[27] Dougherty, E.R., An introduction to morphological image processing, 1992, SPIE Optical Engineering Press.
[28] Kumar S.S., Amutha R., March 30-31, 2012, IEEE international conference on advances in engineering, science and management.
[29] Igbinosa I. E., 2013, International Journal of Information Technology and Electrical Engineering, 2, pp. 25-29.
[30] Shrivakshan G. T., Chandrasekar C., 2012, International Journal of Computer Science, 9, 5, pp. 269-276.
[31] Edelsbrunner H., Mucke E.P., 1994, ACM Trans. Graph., 13, 1, pp. 43-72.
[32] Lafarge T., Pateiro-López B., Possolo A., Dunkers J., 2014, Journal of Statistical Software, 56, 4, pp. 1-17.
[33] Manin, J., Bardi, M., Pickett, L. M., and Payri, R., 2016, International Journal of Multiphase Flow, 83, pp. 267-278, DOI: 10.1016/j.ijmultiphaseflow.2015.12.001



EDITORIAL UNIVERSITAT POLITÈCNICA DE VALÈNCIA